Application of Simplified Numerical and Analytical Methods for Rapid Analysis in Atmospheric Entry Vehicle Design

W. Schuyler Hinman* Craig T. Johansen † and Steven J. Wilson ‡

University of Calgary, Calgary, Alberta, T2N 1N4, Canada

Selected simplified numerical and analytical methods are applied to flow around hypersonic adiabatic blunt bodies. In particular, selected methods that are well defined in the literature, such as the modified Newton's method, transformed finite difference grid in the shock layer, and the method of characteristics in the supersonic region, are utilized to solve the flow around an adiabatic circular cylinder at Mach 6. The results are compared to results obtained by numerical simulation of the compressible Navier-Stokes equations. The comparison is used to draw conclusions about the applicability and accuracy of these methods as they apply to low Reynolds number, small radius of curvature bodies such as atmospheric entry vehicles. A minor improvement to the results is proposed by the inclusion of an iterative interaction between the boundary layer displacement thickness, and the external inviscid free-stream.

Nomenclature

a	Velocity profile parameter, also speed of sound (m/s)
b	Body shape, measured radially from the origin (m)
As	Sutherland constant
C	$\frac{\rho\mu}{\rho_e\mu_e}$
c_p	Specific heat capacity J/(kg K)
c_f	Coefficient of friction
C_p	Coefficient of pressure
F	$F = \frac{U}{U_e}$
G	$G = \frac{H}{H_e}$
H	Total enthalpy (J/kg)
H, J, R, P	Boundary layer integral parameters
m	Slope in boundary layer displacement thickness ($\frac{d\delta^*}{dx}$)
M	Mach number
p	Pressure (Pa)
Pr	Prandtl number
r	Adiabatic recovery factor, also relaxation factor
Re	Reynolds number
$\bar{s}$	Levy-Lees stream-wise coordinate
T	Temperature (K)
T_{aw}	Adiabatic wall temperature (K)
T_s	Sutherland's temperature (K)
U	Tangent velocity component (m/s)
V	Normal velocity component (m/s)
X	Stewartson stream-wise coordinate

*PhD Student, Department of Mechanical Engineering, AIAA Student Member
†Assistant Professor, Department of Mechanical Engineering, AIAA Member
‡MSc. Student, Department of Mechanical Engineering, AIAA Student Member

Y	Stewartson stream-normal coordinate
γ	Specific heat ratio
δ^*	Boundary layer displacement thickness (m)
η	Levy-Lees stream-normal coordinate
θ	Deflection angle
μ	Dynamic Viscosity (kg/ms)
ρ	Density (kg/m^3)
τ	Shear stress (N/m^2)

Subscript

e	Property at boundary layer edge
i	Transformed quantity, also iteration
o	Property at forward stagnation point
w	Property at wall
∞	Free-stream property

I. Introduction

The design of atmospheric entry vehicles, or other high speed blunt-bodies requires an understanding of aerodynamic loads, as well as flow topology. In general, computational fluid dynamics (CFD) simulations of the Navier-Stokes (NS) equations provide the most accurate and detailed predictions of the important flow parameters (drag, lift, control moments, and heating). This is particularly useful when a vehicle geometry is past the initial design phase and more accurate predictions are needed to optimize re-entry trajectory, heating or placement of control mechanisms. However, in the ongoing advancement and development of re-entry vehicles, the shape of the body may be further improved upon by using methods of parametric optimization. This type of optimization would involve evaluating many design variables. In these cases, where the best results are achieved with large sample populations, CFD is an inefficient prediction tool due to the high computational cost.[1,2] Often, significantly simplified methods are used to estimate flow over supersonic blunt bodies.[3] These methods provide fast estimates for flow characteristics in hypersonic flow, however the reduced accuracy of these methods results in reduced confidence in an optimized design result. Historically, the limitation of computer power was a driving force in developing numerical methods resulting in low computational cost.[1,2] The motivation of this present work is to examine some commonly used simplified methods, and compare to CFD results to test their validity and assumptions in the specific case of bodies with a detached bow-shock, and small radius of curvature. As well, a simple method for correcting the inviscid solution due to the weak viscous-inviscid interaction on the body up to but not including the strong interaction region is proposed.

The flow around hypersonic blunt bodies is a mixture of inviscid, and viscous flow. Some methods for solution of the inviscid flow are local surface inclination methods, such as the local tangent cone, modified Newtons method, or shock expansion method.[4] Alternatively the inviscid flow can be solved through direct solution of the Euler equations either numerically, or mathematically.[4–6] In external flows where the radius of curvature is low, and there is no detached bow shock, the surface inclination methods are known to yield reasonably accurate results.[4] However, in the case of a body such as that of an atmospheric entry vehicle, where there is a large subsonic region of flow on the fore-body, and sharp curvature, these methods lose their accuracy. The viscous flow at the wall can be solved either through direct numerical solution of the boundary layer equations, or through integral methods.[4,7] In general, the limitation of using an integral approach to solve the boundary layer equations is the reliance on a predefined family of profiles. As well, boundary layer theory itself comes in to question in flows where the Reynolds number is low, or the streamline curvature is high such as the flow around a body of small radius. Selected methods are briefly described further, and are utilized to predict the flow over an adiabatic cylinder at Mach 6, and various Reynolds numbers ($10^4 < Re < 10^5$). The results are compared to CFD simulation results found in a related parametric study of hypersonic cylinder flow.[8]

It is known that for practical engineering applications, at sufficiently high Reynolds number, the interaction between the viscous boundary layer and the inviscid external flow can be ignored.[9] However, it was shown in a parametric CFD study by the present authors that both Reynolds and Mach number affect the pressure distribution on the body of a supersonic cylinder due to viscous-inviscid interaction by the boundary

layer.[8] Viscous-inviscid interactions can be strong or weak, where strong interactions are usually characterized by separating flow with upstream influence.[1,9] According to Tannehill et. al,[9] in general, the essential elements required to calculate a viscous-inviscid interaction are (1) a method for obtaining the initial and improved inviscid flow solution, (2) a method for solving the boundary layer flow, and (3) a procedure for relating the inviscid and viscous flow solutions that will drive the solution to convergence. Viscous-inviscid interactions in supersonic flow have been characterized by mathematical treatment previously. Some treatments have utilized the parabolic Navier-Stokes equations[1] while others have coupled inviscid and boundary layer solutions.[10–16] The approach presented in this paper utilizes the latter, by solving the external inviscid flow and the boundary layer flow in an iterative fashion. In order to achieve a unique solution for flow around a blunt body shape up to separation such as that of an entry vehicle, the inviscid solution must be capable of handling the subsonic elliptic flow on the fore-body, the supersonic hyperbolic flow past the sonic line, as well the weak viscous-inviscid interaction of the boundary layer.[4] In the present study, a shock-fitted finite difference grid method, as explained in detail by Salas,[6] and Anderson,[4] is used to solve the shock-layer. The rotational method of characteristics is used to complete the formulation of the inviscid flow. The compressible boundary layer equations are solved in the general parabolic form presented by Schetz.[7] The weak interaction of the boundary layer is accounted for by iteratively deforming the shape of the body using a profile of displacement thickness slope ($\frac{d\delta}{dx}$). This formulation is limited to the flow where the interaction is weak, and to two dimensional and axisymmetric flows. The present method to account for weak viscous-inviscid interaction is compared in accuracy to some of the simplified methods above.

The future goal is to formulate a solution method accounting for the entire projectile flow field including the separated region. The present work that ensures a high accuracy solution to the flow prior to separation will be an important part of this as it is known that the separation point, upstream influence, and the pressure rise to separation are determined largely by the incoming boundary layer properties.[17]

II. Description of Numerical and Mathematical Models

A. Inviscid Flow

A.1. Local Surface Inclination Methods (Modified Newton's Method)

The most simple inviscid solutions to the supersonic compressible flow fields are the local surface inclination methods. The modified Newton's method is derived based on Newtonian impact theory and is given in Equation 1. The pressure coefficient utilized in the method is defined in Equation 2. $C_{p_{max}}$ is calculated using the post shock stagnation pressure with Equation 2. θ is the deflection angle from the incoming free-stream flow.

$$C_p = C_{p_{max}} \sin^2 \theta \tag{1}$$

$$C_p = \frac{P - P_\infty}{\frac{1}{2}\rho_\infty V_\infty^2} \tag{2}$$

A major disadvantage of the modified Newton's method is that past a deflection angle of 90 degrees, it is assumed that the pressure coefficient $C_p = 0$. This means that the pressure is assumed to be equal to the free-stream value (See Equation 2). Unfortunately, this limits the applicability of the modified Newton's method to atmospheric entry flows where the flow can remain attached and continue accelerating past 90 degrees.

A.2. Shock-fitted Finite Difference Grid (Elliptic Euler Equations)

On the forebody of the blunt body, the flow is subsonic and the governing Euler equations become elliptic in nature. The governing equations in this region can be solved through a time-stepping, shock-fitted, transformed finite difference grid.[4,6] In standard finite volume solutions the grid extends across shock waves, and complicated numerical techniques are required in order to accurately capture the steep gradients in flow properties. By utilizing shock-fitting techniques, the boundaries of the computational grid are limited to the shock layer. This significantly reduces the computation time by reducing mesh size, and speeds convergence by avoiding complicated shock capturing techniques. The method as explained by both Salas[6] (in cylindrical coordinates), and Anderson[4] (in Cartesian coordinates), utilizes a transformed grid between the shock-wave shape and the body. The use of the transformed finite difference grid is attractive because any body shape

that can be represented by an equation can be solved on a rectangular grid. This also becomes an asset in the proposed weak viscous-inviscid interaction. The basics of this method, as well as the formulation of the transformed governing equations are described in detail by Salas, and Anderson.[4]

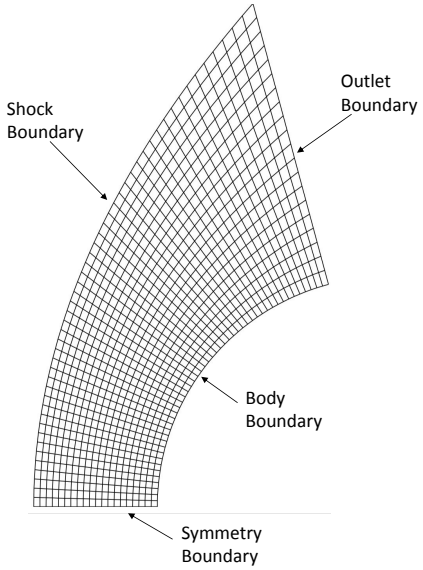

Figure 1. Typical Shock-Fitted Finite Difference Grid

The present method was adapted directly from the sample code provided in the book by Salas.[6] Slight modifications were made to the code to implement thermophysical modelling of gas properties throughout the flow-field (See Section C), and for the curve-fit geometries utilized in the viscous correction. A typical finite difference grid is shown in Figure 1. The grid extends from the shock wave to the body, and from the symmetry plane to the outlet boundary. The solution is achieved by marching forward in time by utilizing the MacCormack finite difference scheme. At each iteration, the gas properties throughout the flowfield are updated using the JANAF polynomial given in Section C. As the solution moves forward in time, all of the properties including the updated gas properties approach convergence. The outlet boundary (See Figure 1) must be placed to ensure that all of the flow is supersonic. This is because the solution method utilizes one-sided backwards difference equations that are only suitable in the hyperbolic nature of supersonic flow. As well, since this time marching finite difference solution is intended to become the input to the method of characteristics solution, it is necessary to ensure that the outlet boundary does not lie adjacent to a characteristic Mach line.

A.3. Method of Characteristics (Hyperbolic Euler Equations)

The method of characteristics is a mathematical method that is useful in solving hyperbolic partial differential equations, such as the supersonic Euler equations. The method solves the flowfield by converting the hyperbolic PDE to a set of algebraic equations that are solved along flow characteristics. Very often, the method of characteristics can be solved assuming irrotational flow, however because the bow shock on a blunt body is curved, entropy and velocity gradients are created across the shock, resulting in rotational flow.[4] Thus, the rotational method of characteristics (RMOC) described by Zucrow and Hoffman was used.[5] In order to solve the rotational method of characteristics the flow is considered isentropic along streamlines. For this type of flow, as described by Anderson[4] and Zucrow and Hoffman,[5] three characteristic lines are required to achieve a solution to the flow field. At any point in the flow field, 4 points are selected, 3 known, and 1 unknown, forming a system of equations that is solved exactly. The derivation of the characteristics and compatibility equations used, as well as detailed descriptions of solution processes, can be found in Zucrow and Hoffman.[5]

A typical characteristics grid resulting from a calculation is shown in Figure 2. The solution is started from an initial value line (calculated with the method in Section A.2) and progressed forward in space until a desired amount of solution is achieved. The characteristic equations are solved iteratively at each

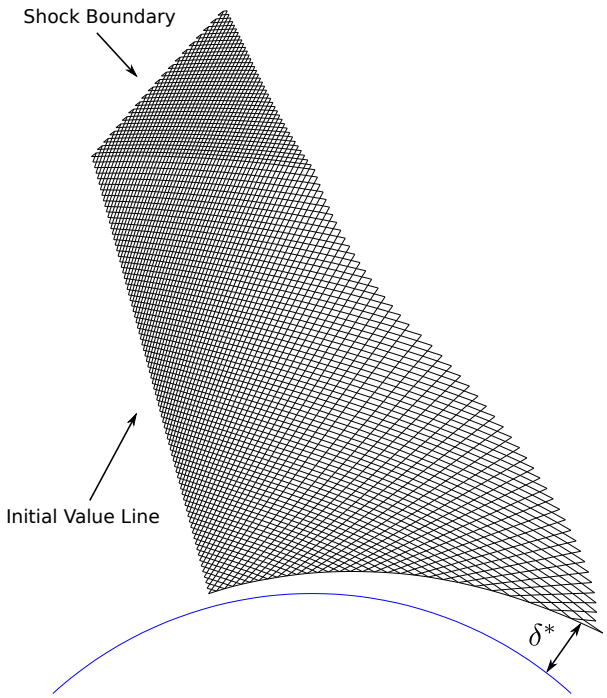

Figure 2. Typical Characteristics Grid

grid intersection. At each iteration, the JANAF polynomial given in Section C is used to update the flow properties, thus facilitating a calculation of the flow field with variable properties. When the local thermodynamics properties are updated, the local Mach angle and speed of sound change, thus impacting the downstream solution. The method of characteristics, similar to the solution to the shock-layer, only requires that the body be represented by an equation. No computational grid needs to be generated or transformed. The output characteristics grid is part of the flow-field solution. In the case for bodies with small radius of curvature (like that of an atmospheric entry vehicle), in order to facilitate solution at points along the wall, a mixture of "direct" and "inverse" wall point methods were required. In the direct wall points, the intersection with the wall of a Mach line emanating from a known internal flow point is calculated. However, on the aft-body it is possible that the Mach line does not intersect the body and therefore cannot be solved. In this case, a point on the wall is selected, and the data in the field is interpolated to find the point in the field where an intersecting Mach line originated. Many improvements to the authors present implementation of the method characteristics can be made, such as to allow the formation of shock-waves in the flow field. As well, in the present implementation of the characteristics grid, the grid is solved from the body to the shock, and steps forward in space in the stream-wise direction. However, not all of the Mach lines emanating from the bow-shock in the supersonic region intersect the body, and therefore do not influence the solution.

B. Viscous Flow

B.1. Integral Momentum Method

A solution of the viscous boundary layer flow can be achieved by simplifying the problem by assuming a set of known similar boundary layer solutions. By integrating the boundary layer equations, and implementing boundary layer thickness parameters the problem of the momentum flow close to the wall can be simplified to a set of ordinary differential equations.[7,15] This has been done in incompressible flows by Thwaites and a similar method for supersonic flows is given by Schetz.[7] A formulation of the integral momentum equations, and set of profile parameters for use in the solution was given by Lees, Reeves, and Klineberg.[14,15,18] The

equations below were obtained from Lees et al. assuming adiabatic flow.[15] This formulation of the boundary layer equations utilizes the Stewartson transformation of the streamwise and normal dimensions (Equation 3 and 4).

$$dX = \left(\frac{p_e a_e}{p_o a_o}\right) dx \tag{3}$$

$$dY = \left(\frac{a_e \rho}{a_o \rho_o}\right) dy \tag{4}$$

$$H\frac{d\delta^*}{dX} + \delta_i^* \frac{dH}{dX} + (2H+1)\frac{\delta_i^*}{M_e}\frac{dM_e}{dX} = \frac{\nu_o}{a_o M_e \delta_i^*} P \tag{5}$$

$$J\frac{d\delta^*}{dX} + \delta_i^* \frac{dJ}{dH}\frac{dH}{dX} + (3J)\frac{\delta_i^*}{M_e}\frac{dM_e}{dX} = \frac{\nu_o}{a_o M_e \delta_i^*} R \tag{6}$$

Equations 5 and 6 are the integral momentum, and moment of momentum equations respectively. In the equations above, R, P, H and J are profile parameters that were evaluated and curve fit to a single profile parameter a by Klineberg and Lees.[14,15,18] In the method of Reeves and Lees, these equations were utilized for strong viscous-inviscid interaction and were coupled with the continuity equation with the Prandtl-Meyer function included to account for displacement of the external inviscid streamline. Here, if we assume that we are solving the boundary layer flow for a known velocity distribution (calculated from an inviscid method), $\frac{dM_e}{dX}$ is known and therefore the continuity equation can be dropped and Equations 5 and 6 are the only necessary equations. A known boundary layer profile is required at the forward stagnation point in order to initialize the solution of the problem. At the stagnation point, the Cohen-Reshotko stagnation profile was utilized.[19] In the present study, these equations were integrated downstream using the 4th order Runge-Kutta technique. The stream-wise derivatives ($\frac{d\delta^*}{dX}$ and $\frac{dH}{dX}$) were solved in a 2×2 matrix to ensure the two equations are directly coupled at each step. The solution results in a distribution of the profile parameters R, P, H J, and a. The shear stress is calculated from the solution by utilizing the shear stress profile parameter P which can be untransformed with Equation 7.

$$\tau_w = \mu_w \left(\frac{M_e\sqrt{\gamma R T_e}}{\delta_i^*}\right)\left(\frac{a_e \rho_w}{a_\infty \rho_\infty}\right) P \tag{7}$$

B.2. Numerical Boundary Layer Solution

The compressible boundary layer equations are parabolic in nature and constitute an initial value problem. In blunt body flows, the solution must be initialized with a stagnation point solution. Similar to the integral method in Section B.1, the Cohen-Reshotko stagnation profile is used.[19] The boundary layer equations are transformed to the Stewartson coordinate system and are given in Equations 8 - 14.[7] When these equations are represented in the general parabolic form (Equation 15) the system of equations is easily discretized and solved using the Crank-Nicolson method. In this form, W represents the unknown variable (F or G) and A_1 to A_4 are constants. All derivatives are approximated using either first order forward or backward, or second order central differences. At each stream-wise step, a tri-diagonal matrix is formed and solved.

$$2\bar{s}F_{\bar{s}} + V' + F = 0 \tag{8}$$

$$2\bar{s}FF_{\bar{s}} + VF' = \beta\left(\frac{\rho_e}{\rho} - F^2\right) + \left(CF'\right)' \tag{9}$$

$$2\bar{s}FG_{\bar{s}} + VG' = \frac{C}{Pr}G'' + \left(\frac{C}{Pr}\right)'G' + \frac{U_e^2}{H_e}\left(\left(1-\frac{1}{Pr}\right)\left(C'FF' + C\left(F'\right)^2 + CFF''\right) + CFF'\left(1-\frac{1}{Pr}\right)'\right) \tag{10}$$

where:

$$F = \frac{u}{U_e} \tag{11}$$

$$G = \frac{H}{H_e} \tag{12}$$

$$C = \frac{\rho\mu}{\rho_e \mu_e} \tag{13}$$

$$\beta = \frac{2\bar{s}}{U_e}\frac{dU_e}{d\bar{s}} \tag{14}$$

$$W'' + A_1 W' + A_2 W + A_3 + A_4 W_{\bar{s}} = 0 \tag{15}$$

Figure 3 presents a diagram illustrating the boundary layer coordinate system, as well as the boundary and initial conditions. The boundary conditions for boundary layer flow are the external flow conditions (determined through solution of the inviscid flow-field) and the conditions at the wall. The present study is focused on the adiabatic wall case. In this case the boundary conditions at the wall are the adiabatic wall temperature and enthalpy, as well as the no-slip condition for velocity. The Prandtl number is calculated using the thermophysical model given in Section C. In order to simplify the solution, the Prandtl number was assumed to be constant at each stream-wise step thus eliminating the derivatives of Prandtl number in the normal direction. The adiabatic wall temperature gives the wall boundary condition and is approximated using the external flow properties and Equation 20. The approximation of an adiabatic wall temperature simplifies the formulation of the equations by providing a boundary condition of G.

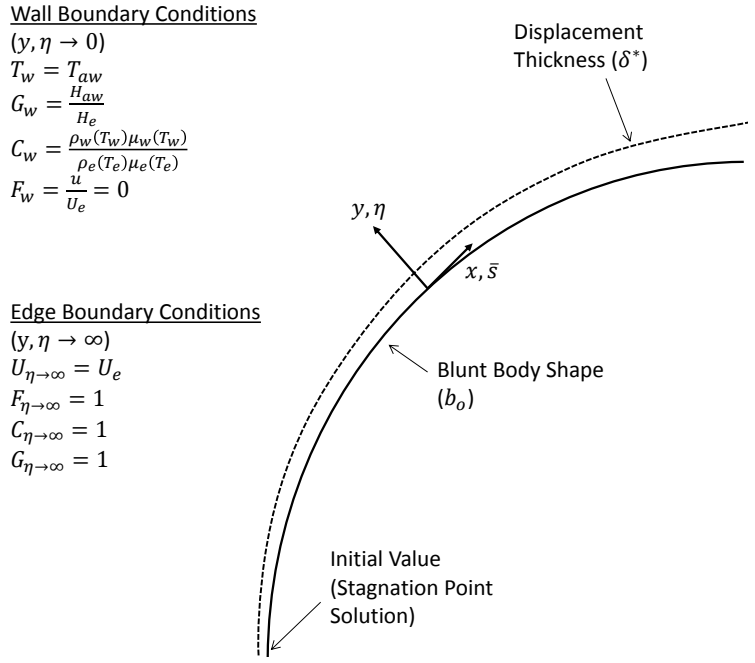

Figure 3. Boundary Layer Solution Set-up

C. Thermophysical Models

In high speed flows, large gradients in temperature exist making an assumption of constant gas properties improper. In order to account for the changing gas properties throughout the flowfield, the gas properties were treated using known models. The specific heat capacity, was modelled using a 7-coefficient JANAF NASA polynomial in the form given in Equation 16.

$$c_p = R(a_1 + a_2 T + a_3 T^2 + a_4 T^3 + a_5 T^4) \tag{16}$$

The viscosity, and thermal conductivity of the fluid was modelled using Sutherland's law. Sutherland's law for viscosity and thermal conductivity is given in Equation 17 and 18. T is the temperature, and C_1 to C_4 are gas constants.[9] The Prandtl number is then calculated with Equation 19. In the previously described boundary layer models, the adiabatic wall temperature is approximated by Equation 20 from Shetz.[7]

$$\mu = C_1 \frac{T^{1/2}}{T + C_2} \tag{17}$$

$$k = C_3 \frac{T^{1/2}}{T + C_4} \tag{18}$$

$$Pr = \frac{\mu c_p}{k} \tag{19}$$

$$T_{aw} = T_e + r\frac{U_e^2}{2c_p} = T_e + Pr^{0.5}\frac{U_e^2}{2c_p} \tag{20}$$

III. Weak-Interaction Solution

The previous sections briefly described well defined methods that on their own provide solutions to either the inviscid, or viscous flow. In reality, there is a weak viscous-inviscid interaction between the boundary layer and the external inviscid free-stream. At high Reynolds numbers, this effect can be small, but at low Reynolds numbers the effect can be large. Re-entry vehicles operate at high altitudes where (assuming the flowfield is still a continuum) the viscous-inviscid interaction on the body can be significant. Here, a simple method where the prediction of the flow around the body is corrected for this interaction is proposed. The main goal is to examine and evaluate the increase in accuracy at various Reynolds numbers. In order to join the viscous and inviscid solutions together, an iterative approach is required that will cause the error between iterations to disappear. To accomplish this, it is assumed that the effect of the boundary layer on the external flow can be quantified by the displacement thickness (δ^*). Because of the solution from the shock layer does not join entirely smoothly to the method of characteristics, the these two regions are solved separately. Initially, the inviscid solution to the shock-layer is solved for the actual body shape (b_o). The boundary layer is then solved using the conditions predicted from the inviscid solution as the edge boundary conditions that are represented by polynomial functions. The calculated displacement thickness (Equation 21) is added to the body in the normal direction. The new body is represented by a polynomial fit, and used to repeat the shock-layer solution. This process is repeated until convergence. Between iterations, the successive displacement of the body is calculated using the error in the displacement thickness between iterations (Equation 23).

$$\delta^* = \int_0^\infty \left(1 - \frac{\rho u}{\rho_e u_e}\right) dy = \frac{\sqrt{2\bar{s}}}{\rho_e u_e} \int_0^\infty \left(\frac{\rho_e}{\rho} - F\right) d\eta \tag{21}$$

$$\Delta\delta_i^* = \delta_i^* - \delta_{i-1}^* \tag{22}$$

$$b_i = b_{i-1} + \Delta\delta_i^* \tag{23}$$

The above solution method was found to work well and lead to fast convergence for the shock-layer, however, due to the sensitivity of supersonic flow to small perturbation in body shape, a slightly different convergence method was used for the rest of the body. Specifically, the use of the magnitude of displacement thickness as the iterative variable is not suitable. In supersonic flow the change in external streamline angle, and thus $\frac{d\delta^*}{dx}$, is important in predicting stream-wise properties. For flows where M>1 this can be represented using simple free-interaction theory (Equation 24).[17] Because of this, a simple convergence approach based on $\frac{d\delta^*}{dx}$ was made.

$$\frac{\sqrt{M^2 - 1}}{\gamma M^2}\frac{\Delta p}{p} = \Delta\psi = \arctan\left(\frac{d\delta^*}{dx}\right) \tag{24}$$

From the converged solution of the shock-layer and the boundary layer on the fore-body, the initial boundary layer properties, and an initial value line for the method of characteristics are known. In the first iteration, a constant value of ($m = \frac{d\delta^*}{dx}$) is assumed. With this, an initial guess for the deformed body is calculated. The characteristics mesh is then evaluated using this body shape. Using the solution found from the characteristics, a new corrected body shape is determined. The error between the previous iterations

result for the profile of displacement thickness is used to predict the next iterations profile (Equation 25 to 28). A combination of spline and polynomial fits are used in order to pass the external flow variables to the boundary layer solution, and the body shape to the inviscid solution. In order to ensure a stable solution, the streamline angle was restricted to a low order polynomial. If a spline, or direct interpolation was used, small changes in the shape of the body eventually led to divergence. This somewhat restricts the solution, but ensures convergence.

$$\Delta m_i = m_{calc} - m_{i-1} \tag{25}$$

$$m_i = m_{i-1} + r \times \Delta m_i \tag{26}$$

$$\delta_i^*(x) = \delta_o^* + \int m_i dx \tag{27}$$

$$b_i = b_o + \delta_i^* \tag{28}$$

An important detail of the method shown in Equations 25 to 28 is the relaxation factor r. Difficulty in convergence was present at low Reynolds number. In order to stabilize the method, the iteration process is under-relaxed. This is a common requirement in methods of viscous-inviscid interaction.[9] The convergence for the supersonic region of the flow around an adiabatic cylinder at Mach 6, and a Reynolds number of $Re = 5 \times 10^4$ is shown in Figure 4. Here, the % error is calculated as the maximum % difference of flow properties between iterations. The result shown is typical of other test cases examined.

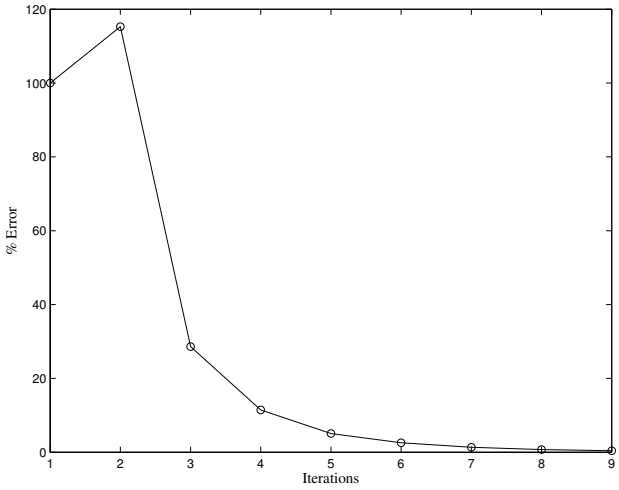

Figure 4. Typical Convergence Trend

IV. CFD Set-up

The methods briefly discussed in Sections (II and III) are compared to simulation results obtained in a related study by the present authors.[8] The simulation was performed using the open-source CFD software OpenFOAM. In particular, the density based compressible flow solver, rhoCentralFoam, was used. The simulations were performed assuming continuum, equilibrium, and laminar flow. The thermophysical modelling implemented in the solver are the Sutherland, and JANAF models described in Section C. The governing equations solved in rhoCentralFoam are the compressible Navier-Stokes equations (Equation 29 to 31).[20]

$$\frac{\partial \rho}{\partial t} + \nabla \cdot (\rho u) = 0 \tag{29}$$

$$\frac{\partial (\rho u)}{\partial t} + \nabla \cdot (\rho u^2) - \nabla p - \nabla \cdot \tau = 0 \tag{30}$$

$$\frac{\partial \rho E}{\partial t} + \nabla \cdot (u(\rho E)) + \nabla \cdot [up] + \nabla \cdot (\tau \cdot u) + \nabla \cdot j = 0 \tag{31}$$

where ρ, u, p, j, and τ represent the density, velocity, pressure, diffusive heat flux, and viscous stress tensor respectively. The central discretization scheme used by rhoCentralFoam makes it less susceptible to spurious numerical oscillations at strong flow discontinuities such as shockwaves.[20,21] This makes rhoCentralFoam an appropriate solver in the present case because of the strong bow shock and density gradients present in the flow.

The simulation was performed on a mesh-independent grid consisting entirely of unstructured hexahedral elements. The inlet boundary conditions were set with constant P, T, and U. The outlet boundary conditions were all treated as zero-gradient for all properties. The Mach and Reynolds number of the flow were controlled by fixing the inlet temperature, and manipulating the pressure and velocity. A schematic of the grid is shown in Figure 5.

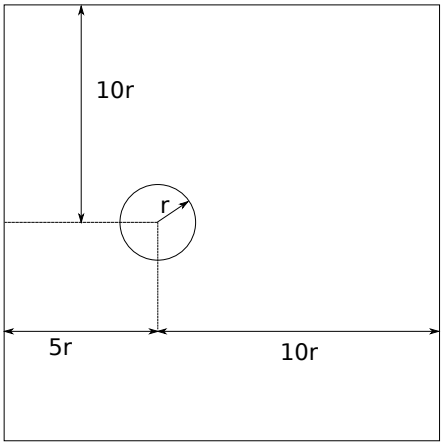

Figure 5. Simulation Domain

The results of the simulation were compared to experiments performed at Mach 5.75 by McCarthy et. al and showed close agreement for pressure distribution.[8,22] A parametric study of the effect of free-stream Mach and Reynolds number on flow properties was performed. Because of the good accuracy of representative simulations compared to experiment, simulation results at various Reynolds numbers are used as a bench mark in the present study. A typical simulation result is shown by a synthetic Schlieren image in Figure 6.

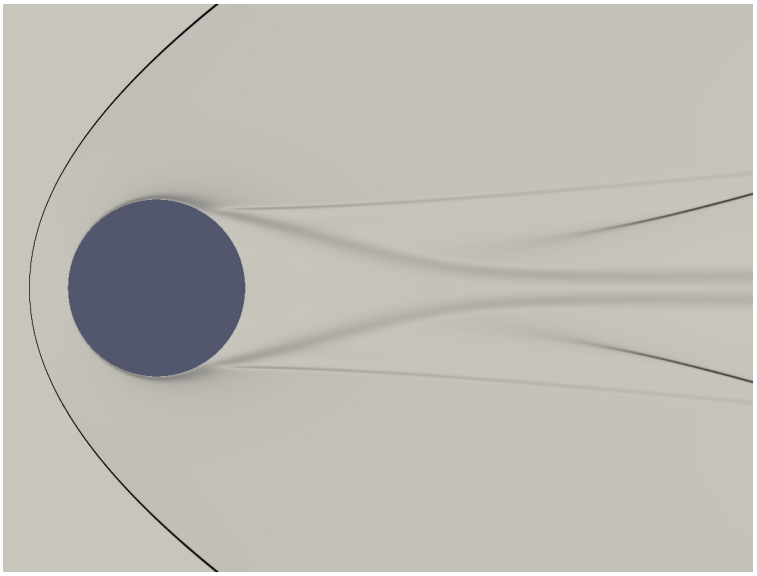

Figure 6. Typical CFD Result($M = 6$, $Re = 50000$)

V. Results and Discussion

In Figure 7, the pressure distribution along the surface of an adiabatic cylinder predicted from several methods is compared. The modified Newton's method (Section A.1), the solution to the Euler equations by a joining between a finite difference grid and a characteristics mesh (Section A.2 and A.3) and the present simple approach including the correction for weak viscous-inviscid interaction (Section III) are compared against the rhoCentralFoam results.

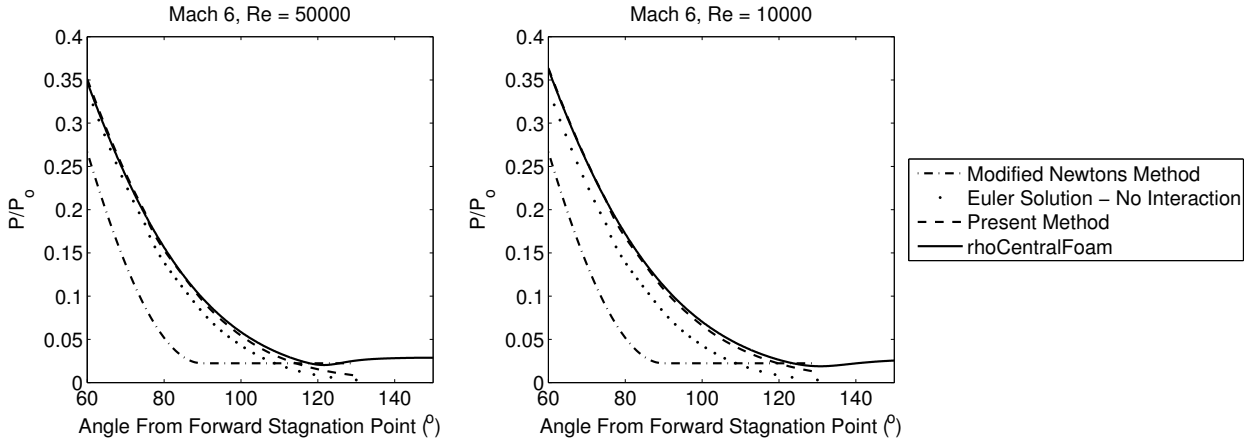

Figure 7. Pressure Distribution

The results for pressure distribution are normalized to the predicted stagnation pressure at the fore-body stagnation point. Figure 7 shows the results for two representative Reynolds numbers. The results show close agreement between the laminar Navier-Stokes simulation and the weak interaction approach approximately up to the pressure minima for both Reynolds numbers. After the pressure minima, the interaction between the viscous flow and the external inviscid flow becomes strong and requires special treatment. The results of the Euler equations without any modification for the interaction still show close results to the CFD solution. In the high Reynolds number case, it is clear that less advantage was gained in prediction of the pressure distribution by accounting for the interaction. At a Reynolds number of $Re = 10^4$, the change in the pressure distribution due to the viscous interaction calculation is noticeable. The modified Newtons method shows reasonable accuracy on the forebody close to the stagnation point (angles less than 60^o not shown in figure) however, the error in the prediction increases downstream. In particular, the results show that in the case of a re-entry body, where the deflection angle from the freestream is $< 90^o$, the prediction for pressure distribution is poor. A summary of the effect of Reynolds number, and the relative accuracy of each method

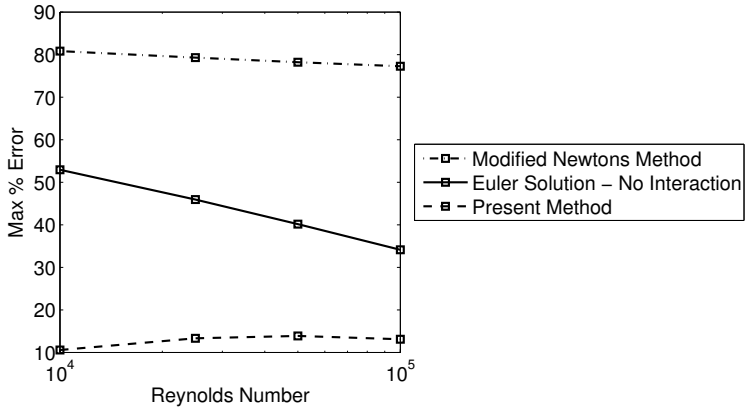

Figure 8. Max % Error in Normalized Pressure (P/P_o)

is shown in Figure 8. The plot shows the maximum percent error in normalized pressure between 0 and 110 degrees. The % error is calculated between the predicted and the rhoCentralFoam results. It is clear that at

all Reynolds numbers, the correction for viscous interaction leads to a significant improvement in accuracy for the prediction of pressure distribution. At a Reynolds number of $Re = 10^4$, the error reduced from approximately 50% to 10% when the solution to the Euler equations was corrected for the viscous-inviscid interaction. At a Reynolds number of $Re = 10^5$ the reduction in error is less significant but still yields improved accuracy. This justifies the use of the present method of correction throughout the investigated Reynolds number range. The modified Newton's method has large error and only mildly increases in accuracy with Reynolds number. The Euler solution gives more accurate results than the modified Newton's method, and the error reduces noticeably with increasing Reynolds number.

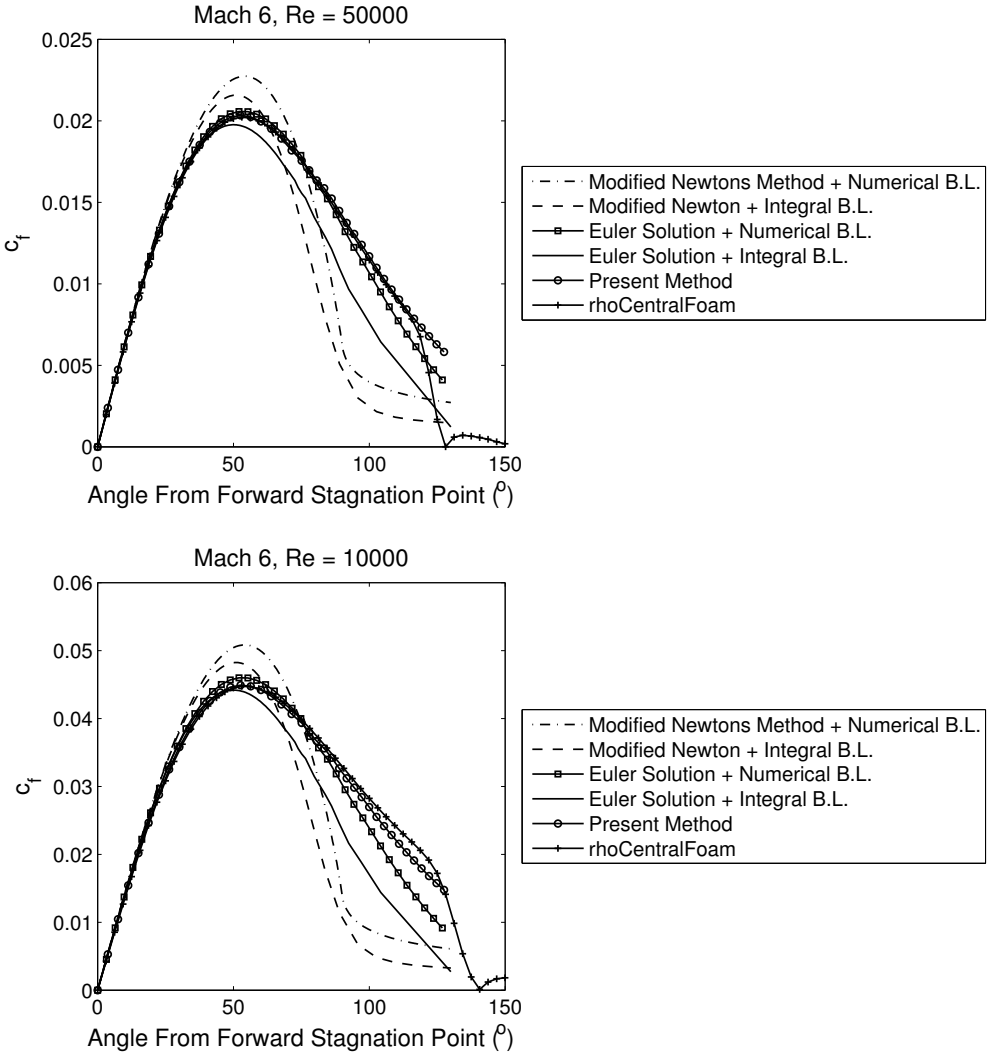

Figure 9. Coefficient of Friction

To assess the accuracy and applicability of the boundary layer methods described in Section B, the shear stress was compared along the surface of the adiabatic cylinder. In Figure 9, the coefficient of friction $c_f = \frac{\tau_w}{0.5\rho_\infty U_\infty^2}$ is plotted as a function of angle from the forward stagnation point. The results were compared for different combinations of inviscid and viscous solutions, as well as with and without the interaction method presented in Section III. The results for shear stress lead to similar conclusions regarding the applicability of the methods as the results for pressure distribution. Variations in the external flow properties influence the development of the boundary layer. Therefore the quality of the boundary layer solution is not only a function of the applicability of the assumptions in the governing equations, but also by the quality of the solution for the boundary conditions (P_e, U_e, M_e, T_e, T_{aw} and μ_w). Using the modified Newton's method for the external flow parameters, the results from the integral momentum method, and the numerical solution of the compressible boundary layer equations were compared. The results show that the correct shape for

the shear stress profile are found, however the magnitude of the coefficient of friction is over-predicted in both cases. The most error between the modified Newton's method boundary layer predictions was for the integral momentum method. Past 90^o, where the pressure is assumed constant, the solution shows poor results.

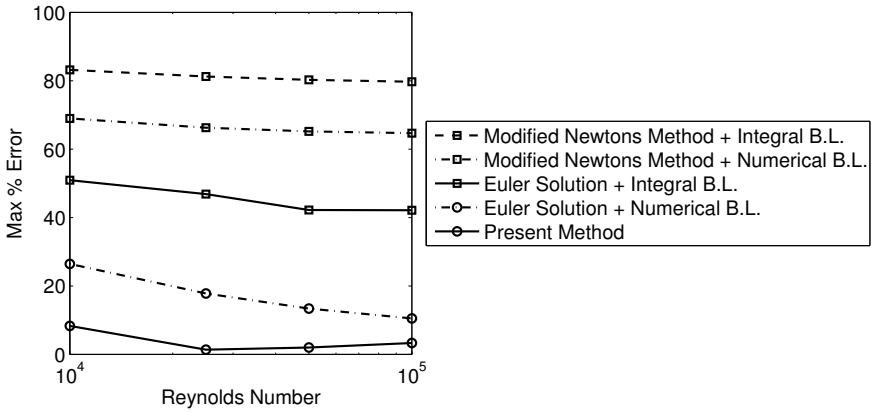

Figure 10. Max % Error in Coefficient of Friction (C_f)

Using the solutions based on the Euler equations to give the external flow parameters, all of the results show improved agreement to the CFD. The solution given by the integral momentum method shows an improvement for the distribution of shear stress, however the peak magnitude of c_f is under-predicted, particularly on the aft-body. The reduced accuracy of the integral method is due to the restriction of the solution to a family of boundary layer profiles, in this case the Klineberg[18] polynomials. The Euler solution to the inviscid flow, with the numerical solution of the boundary layer equations shows good results for shear stress distribution along the body. The predictions match closely up to 90 degrees but have increasing error on the aft-body. This is because as the flow expands around the cylinder, the favorable pressure gradient induces boundary layer growth, which then acts to alter the pressure distribution. This is shown in the pressure distribution results previously discussed. The improvement of the solution by implementing the weak interaction correction given in Section III is seen in the results for shear stress. At high Reynolds number, the corrected shear stress closely matches the CFD results. At low Reynolds number, the improvement is also clear, however, the error is not reduced as significantly. A summary of the accuracy of each method in the Reynolds number range investigated is shown in Figure 10. The maximum % error in coefficient of friction between 0 and 110 degrees is plotted. The % error is calculated between the predicted and the rhoCentralFoam results. The increased accuracy of the numerical boundary layer solution is evident. For the present method, the error in coefficient of friction is $< 10\%$ throughout the range of Reynolds numbers investigated. The gains in accuracy of the interaction solution are reduced as Reynolds number is increased, and the accuracy of the solution neglecting interaction is improved.

VI. Conclusions and Future Work

Simple analytical and numerical methods were used to calculate and estimate pressure and shear stress distributions along an adiabatic cylinder at Mach 6, and various Reynolds numbers, up to the pressure minima. A simple method for accounting for the weak viscous-inviscid interaction between the boundary layer and the external free-stream was given. The results were compared to those obtained from the numerical simulation of the compressible Navier-Stokes equations. The analysis was performed in the context of evaluating each methods merits to be used for the rapid design and analysis of atmospheric entry vehicles. Atmospheric entry vehicles, in general, have low radius of curvature and often fly at low Reynolds numbers and thus specific attention must be given to analytical prediction of flow properties. The results showed that a specific surface inclination method (the modified Newton's method) is not suitable because of its poor accuracy away from the forward stagnation point. A solution to the Euler equations using a shock-fitted finite difference grid on the fore-body joined to a characteristics grid in the supersonic free-stream showed close agreement to the CFD at higher Reynolds numbers. The integral boundary layer method utilizing the single parameter family of profiles from Klineberg,[18] and Lees and Reeves,[15] was found to under predict the

shear stress around the body. The general parabolic solution to the compressible boundary layer equations showed close agreement to the CFD results. The results from the simple viscous-inviscid interaction solution showed improved accuracy from the calculations where the interaction was ignored. However, at low Reynolds numbers, error still existed between the predicted shear stress and the shear stress predicted by the CFD.

A long term goal of the present study is to find the best simplified solution method for the rapid design and analysis of atmospheric entry vehicles that can be used in design optimization algorithms of 2D and axi-symmetric re-entry shapes. The near-wake of re-entry bodies presents many challenges in design and analysis. Future work will focus on reviewing new and historical approaches to the treatment of the near-wake for use in rapid design and analysis. While CFD solutions to the complete compressible Navier-Stokes equations offer the most accuracy, it is believed by the present authors that the high cost of CFD simulations demands renewed interest in the simplified models developed in the past.

References

[1]Barnett, M. and Davis, R. T., "Calculation of Supersonic Flows with Strong Viscous-Inviscid Interaction," *AIAA Journal*, Vol. 24, No. 12, Dec. 1986, pp. 1949–1955.

[2]Inger, G. V., "Analytical Treatment of Shock Wave-Boundary-Layer Interactions," *Shock Wave-Boundary Layer Interactions*, edited by H. Babinsky and J. K. Harvey, chap. 10, Cambridge University Press, New York, NY, 1st ed., 2011, pp. 395–457.

[3]Rodi, P., "Optimization of Bezier Curves for High Speed Leading Edge Geometries," *51st AIAA Aerospace Sciences Meeting including the New Horizons Forum and Aerospace Exposition*, American Institute of Aeronautics and Astronautics, Grapevine (Dallas/Ft. Worth Region), Texas, Jan. 2013.

[4]Anderson, J. D., *Hypersonic and High-Temperature Gas Dynamics*, American Institute of Aeronautics and Astronautics, Blacksburg, Virginia, 2nd ed., 2006.

[5]Zucrow, M. J. and Hoffman, J. D., *Gas Dynamics Vol. 2*, John Wiley and Sons, 1977.

[6]Salas, M. D., *A Shock-Fitting Primer*, Taylor & Francis Group, LLC, Bova Raton, FL, 2010.

[7]Schetz, J. A., *Boundary Layer Analysis*, Prentice Hall, Upper Saddle River, New Jersey, 1st ed., 1993.

[8]Hinman, W. S. and Johansen, C. T., "Numerical Investigation of Laminar Near Wake Separation on Circular Cylinders at Supersonic Velocities," *29th Congress of the International Council of the Aeronautical Sciences*, International Council of the Aeronautical Sciences, St. Petersburg, Russia, 2014, pp. 1–10.

[9]Tannehill, J. C., Anderson, D. A., and Pletcher, R. H., *Computational Fluid Mechanics and Heat Transfer 2nd Ed.*, Taylor & Francis, 1997.

[10]Doss, E. D., Dwyer, H. A., and Goldman, A., "Rapid Calculation of Inviscid and Viscous Flow Over Arbitrary Shaped Bodies," *Journal of Aircraft*, Vol. 8, No. 2, Feb. 1971, pp. 125–127.

[11]Reyhner, T. A. and Hickcox, T. E., "Combined Viscous-Inviscid Analysis of Supersonic Inlet Flowfields," *Journal of Aircraft*, Vol. 9, No. 8, Aug. 1972, pp. 589–595.

[12]Johnston, W. and Sockolf, P., "Matching Procedure for Viscous-Inviscid Interactive Calculations x," *AIAA Journal*, Vol. 17, No. 6, June 1979, pp. 661–663.

[13]Grange, J.-m., Klineberg, J. M., and Lees, L., "Laminar Boundary-Layer Separation and Near-Wake Flow for a Smooth Blunt Body at Supersonic and Hypersonic Speeds," *AIAA Journal*, Vol. 5, No. 6, 1967, pp. 1089–1096.

[14]Reeves, B. L. and Lees, L., "Theory of Laminar Near Wake of Blunt Bodies in Hypersonic Flow," *AIAA Journal*, Vol. 3, No. 11, 1965, pp. 2061–2074.

[15]Lees, L. and Reeves, B. L., "Supersonic Separated and Reattaching Laminar Flows: I. General Theory and Application to Adiabatic Boundary- Layer/Shock-Wave Interactions," *AIAA Journal*, Vol. 2, No. 11, 1964, pp. 1907–1920.

[16]Miller, G., "Mathematical Formulation of Viscous-Invsicid Interaction Problems in Supersonic Flow," *AIAA Journal*, Vol. 11, No. 7, 1973, pp. 938–942.

[17]Delery, J., "Physical Introduction," *Shock Wave-Boundary Layer Interactions*, edited by H. Babinsky and J. K. Harvey, chap. 2, Cambridge University Press, New York, NY, 1st ed., 2011, pp. 5–86.

[18]Klineberg, J. M. and Lees, L., "Theory of Laminar Viscous-Inviscid Interactions in Supersonic Flow," *AIAA Journal*, Vol. 7, No. 12, 1969, pp. 2211–2221.

[19]Cohen, C. and Reshotko, E., "Similar Solutions for the Compressible Laminar Boundary Layer with Heat Transfer and Pressure Gradient (Rept. 1293)," Tech. rep., N.A.C.A., 1956.

[20]Greenshields, C. J., Weller, H. G., Gasparini, L., and Reese, J. M., "Implementation of Semi-discrete, Non-staggered Central Schemes in a Colocated, Polyhedral, Finite Volume Framework, for High-speed Viscous Flows," *International Journal for Numerical Methods in Fluids*, 2009, pp. n/a–n/a.

[21]Arisman, C., Johansen, C. T., Galuppo, W., and McPhail, A., "Nitric Oxide Chemistry Effects in Hypersonic Boundary Layers," *43rd Fluid Dynamics Conference*, American Institute of Aeronautics and Astronautics, Reston, Virginia, June 2013.

[22]McCarthy, J. F. and Kubota, T., "A Study of Wakes Behind a Circular Cylinder at M Equal 5.7," *AIAA Journal*, Vol. 2, No. 4, April 1964, pp. 629–636.